

6. CONCLUSION

A tri-band BPF with controllable bandwidths is presented based on stub-loaded SIRs. The proposed tri-band BPF has the advantage of the independent control for the three bandwidths. The first and second bandwidths are designed using two coupling paths, while the third bandwidth is designed by adjusting the dimensions of the open-stub. The proposed filter also has the compact size. The rejection level between the first and second passbands will be enhanced by introducing an additional open-stub.

ACKNOWLEDGMENT

This research was supported by the KCC (Korea Communications Commission), Korea, under the R&D program supervised by the KCA (Korea Communications Agency) (KCA-2012-12-911-01-101).

REFERENCES

1. C.-F. Chen, T.-Y. Huang, and R.-B. Wu, Design of dual- and triple-passband filters using alternately cascaded multiband resonators, *IEEE Trans Microwave Theory Tech* 54 (2006), 3550–3558.
2. Q.-X. Chu, X.-H. Wu, and F.-C. Chen, Novel compact tri-band bandpass filter with controllable bandwidths, *IEEE Microwave Wireless Compon Lett* 21 (2011), 655–657.
3. C.-H. Lee, C.-I. G. Hsu, and H.-K. Jhuang, Design of a new tri-band microstrip BPF using combined quarter-wavelength SIRs, *IEEE Microwave Wireless Compon Lett* 16 (2006), 594–596.
4. X.-Y. Zhang, Q. Xue, and B.-J. Hu, Planar tri-band bandpass filter with compact size, *IEEE Microwave Wireless Compon Lett* 20 (2010), 262–264.
5. X. Lai, C.-H. Liang, H. Di, and B. Wu, Design of tri-band filter based on stub loaded resonator and DGS resonator, *IEEE Microwave Wireless Compon Lett* 20 (2010), 265–267.
6. C.-I.G. Hsu, C.-H. Lee, and Y.-H. Hsieh, Tri-band bandpass filter with sharp passband skirts designed using tri-section SIRs, *IEEE Microwave Wireless Compon Lett* 18 (2008), 19–21.
7. W.-Y. Chen, M.-H. Weng, and S.-J. Chang, A new tri-band bandpass filter based on stub-loaded step-impedance resonator, *IEEE Microwave Wireless Compon Lett* 22 (2012), 179–181.
8. Q.-X. Chu, F.-C. Chen, Z.-H. Tu, and H. Wang, A new tri-band bandpass filter based on stub-loaded step-impedance resonator, *IEEE Trans Microwave Theory Tech* 57 (2009), 1753–1759.
9. H. Chen, High isolation tri-band BPF using tri-mode resonator, *Microwave Opt Technol Lett* 55 (2013), 1367–1370.
10. B.A. Syrett, A broad-band element for microstrip bias or tuning circuits, *IEEE Trans Microwave Theory Tech* 28 (1980), 925–927.

© 2014 Wiley Periodicals, Inc.

A MODELING METHOD FOR DUMBBELL-SHAPED DGS AND ITS PARAMETER EXTRACTION

Duk-Jae Woo,¹ Taek-Kyung Lee,² and Sangwook Nam¹

¹Institute of New Media & Communications, The School of Electrical Engineering and Computer, Science/Electrical Engineering, Seoul National University, Gwanak-gu, Seoul

²School of Electronics, Telecommunication, and Computer Engineering, Korea Aerospace University, Goyang-si, Gyeonggi-do, South Korea; Corresponding author: tklee@kau.ac.kr

Received 10 April 2014

ABSTRACT: This article presents an equivalent circuit model for a dumbbell-shaped defected ground structure (DGS) in a microstrip line. The effects of equivalent circuit elements of a dumbbell-shaped DGS

and their magnetic coupling to the host transmission line are modeled as a simple lumped-element circuit. By adding a virtual capacitor on the narrow etched gap, the values of inductance and capacitance of the dumbbell-shaped DGS in the ground plane were extracted. Also, other main circuit parameters of the proposed circuit model were extracted using EM simulation result. This article provides one approach for understanding the operating principle of the DGS structures. © 2014 Wiley Periodicals, Inc. *Microwave Opt Technol Lett* 56:2910–2913, 2014; View this article online at wileyonlinelibrary.com. DOI 10.1002/mop.28736

Key words: defected ground structure; equivalent circuit model; magnetic coupling

1. INTRODUCTION

In recent years, there has been an increasing interest in planar transmission lines with various defected ground structures (DGSs) that prohibit wave propagations in certain frequency bands. These structures exhibit advantages, such as ease of fabrication and compatibility with monolithic microwave integrated circuits. DGSs have been effectively used to improve the performance of a wide range of microwave circuits such as: planar resonators, filters, antennas, power amplifiers, or power dividers [1–4]. In those applications, the key issue is to obtain a simple and accurate circuit model to attain optimized design with an aimed performance. Some equivalent circuit models have been presented and these efforts have provided improved design methods and physical insight into the operation principle of the DGSs [1,2,5–11].

Because of its wide-band rejection properties, DGSs with a dumbbell shape are popularly used in the suppression of undesired harmonics for microwave circuits and in the design of low-pass filters. In this article, we suggest a new equivalent circuit model for a dumbbell-shaped DGS coupled to a transmission line, especially a microstrip line, to provide one approach to understand the electromagnetic behavior of DGS structures. In addition, we propose a method to extract the main circuit parameter values of the proposed circuit model.

2. EQUIVALENT CIRCUIT MODEL

Figure 1 illustrates the geometry of the microstrip line with a dumbbell-shaped DGS, where two circular etched areas are connected by a narrow etched gap. In the DGS in the ground plane,

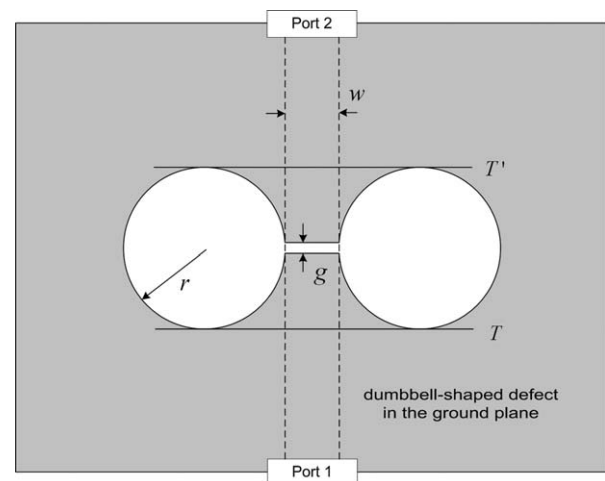


Figure 1 Configuration of microstrip line with a dumbbell-shaped DGS

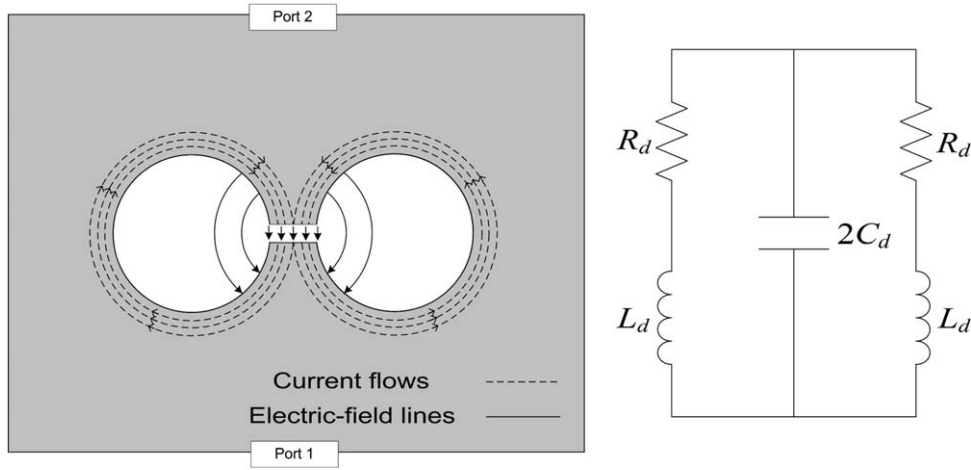


Figure 2 Sketch of the current flows and electric field lines for the dumbbell-shaped DGS in the ground plane of the microstrip line and its equivalent circuit model

as shown in Figure 2(a), the electric field is concentrated around the narrow etched gap, while the current is confined to the metallic ground plane surrounding the circular etched pattern. The DGS in the ground plane can therefore be represented by an RLC resonant circuit model as shown in Figure 2(b). From the symmetry of the structure, R_d , L_d , and C_d are the resistance, the inductance and the capacitance of the half of DGS in the ground plane divided by the plane of symmetry along the center of the microstrip line.

For the dumbbell-shaped DGS loaded microstrip line, the equivalent circuit model can be proposed as illustrated in Figure 3(a) [11]. The magnetic flux from the current on the host transmission line passes through the wide etched circular area on the ground plane and it causes a magnetic coupling of the DGS to the host line. The L_m represents the mutual inductance coupling the DGS to the host line. The mutual inductance can be given by $L_m = k_m \sqrt{L_0 L_d}$, where k_m is the coupling coefficient between the host transmission line and the resonator [11]. Here, the L_0 and C_0 are the inductance and capacitance of the microstrip transmission line corresponding to the length occupied by a DGS, respectively. Also, near the resonance frequency, we can express the simplified equivalent circuit model as shown in Figure 3(b). The expressions

for the inductance, the capacitance, and the resistance of the simplified equivalent circuit are given by

$$L = 2\omega_0^2 L_m^2 C_d = 2k_m^2 L_0, \quad (1)$$

$$C = L_d / (2\omega_0^2 L_m^2) = L_d C_d / (2k_m^2 L_0) = L_d C_d / L, \quad (2)$$

$$R = 2\omega_0^2 L_m^2 / R_d = 2k_m^2 L_0 / (R_d C_d), \quad (3)$$

respectively, with a resonance angular frequency of $\omega_0 = 1 / \sqrt{L_d C_d} = 1 / \sqrt{LC}$.

3. EQUIVALENT CIRCUIT PARAMETER EXTRACTION

One of the objectives in this letter is to find the parameter values (L_d , C_d , R_d , and k_m) of the proposed equivalent circuit model in Figure 3(a). The inductance L_0 and the capacitance C_0 of the microstrip transmission line, corresponding to the length occupied by a DGS, can be easily obtained from the analytical expression in [12].

To find the values of the inductance L_d and the capacitance C_d , we present a DGS which is loaded by an additional virtual capacitance C_r , as shown in Figure 4. The equivalent circuit model is also illustrated in Figure 4. As the resonance frequencies for unloaded and loaded DGSs are $f_0 = 1 / (2\pi \sqrt{L_d C_d})$ and $f_{0r} = 1 / (2\pi \sqrt{L_d (C_d + C_r / 2)})$, respectively, we can obtain L_d and C_d by comparing two resonance frequencies:

$$L_d = \frac{1}{2C_r \pi^2} \left(\frac{1}{f_{0r}^2} - \frac{1}{f_0^2} \right), \quad C_d = \frac{1}{4\pi^2 f_0^2 L_d}. \quad (4)$$

Also, we can find the values of resistance R_d and coupling coefficient k_m using the results of EM simulation. From the simulation results of the scattering parameter near the resonance frequency, the circuit parameters of the resonator in Figure 3(b) are determined, respectively [2]:

$$L = 2Z_0 (1/\omega_c - \omega_c/\omega_0^2), \quad (5)$$

$$C = 1/(\omega_0^2 L), \quad (6)$$

$$R = 2Z_0 / \left(\frac{1}{|S_{11}(\omega_0)|} - 1 \right). \quad (7)$$

Here, ω_0 is the angular resonance frequency, ω_c is the 3 dB cutoff angular frequency, and Z_0 is the characteristic impedance of the microstrip line.

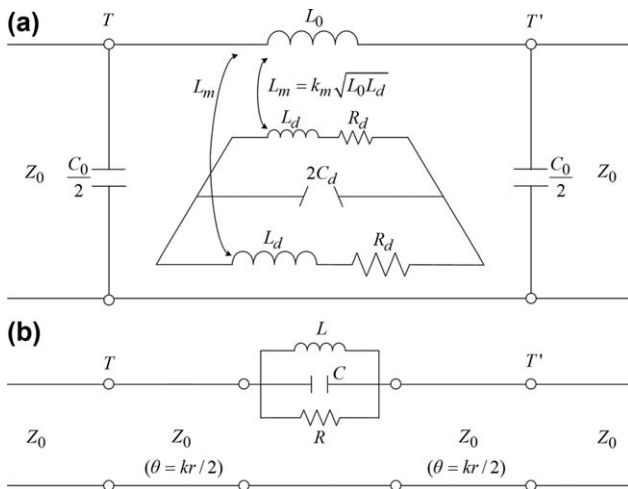


Figure 3 (a) Lumped element equivalent circuit model for a microstrip line with a dumbbell-shaped DGS. (b) Simplified equivalent circuit of the branch between T and T'

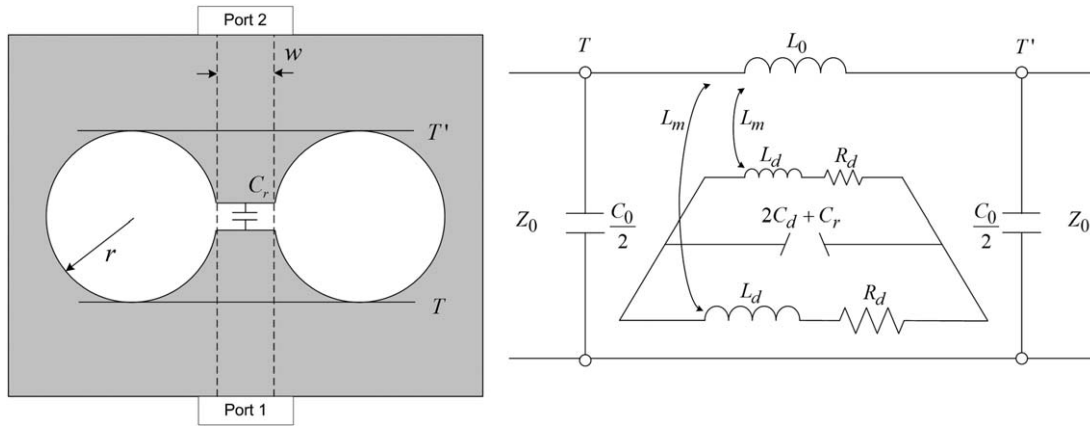


Figure 4 Topology of DGS loaded with capacitance C_r and its equivalent circuit model

TABLE 1 Extracted Circuit Parameters for Various radii of the Etched Circular Pattern ($C_r = 0.1$ pF)

r (mm)	L_0 (nH)	C_0 (pF)	f_0 (GHz)	f_{0r} (GHz)	f_c (GHz)	S_{11} (dB)	L (nH)	C (pF)	R (Ω)	k_m	L_d (nH)	C_d (pF)	R_d (Ω)
2.0	1.708	0.708	6.56	5.20	4.36	-0.742	2.002	0.294	1101	0.766	6.963	0.085	21
2.5	2.135	0.885	5.54	4.50	3.50	-0.633	2.685	0.307	1299	0.793	8.511	0.097	21
3.0	2.562	1.061	4.85	3.97	2.93	-0.594	3.390	0.318	1388	0.813	10.606	0.102	24
3.5	2.989	1.238	4.34	3.59	2.48	-0.573	4.264	0.315	1442	0.845	12.412	0.108	27
4.0	3.416	1.415	3.93	3.27	2.19	-0.553	4.924	0.333	1495	0.849	14.577	0.113	29
4.5	3.843	1.592	3.6	3.02	1.91	-0.573	5.883	0.332	1441	0.875	16.456	0.119	34
5.0	4.270	1.769	3.33	2.81	1.71	-0.605	6.734	0.339	1361	0.888	18.473	0.124	40

Using the defined parameters, the resistance R_d can be easily obtained. From (3), the resistance R_d is given by

$$R_d = 2k_m^2 L_0 / (RC_d) = L / (RC_d), \quad (8)$$

where, L , R , and C_d were defined in (5), (7), and (4), respectively. Also, by comparing (1) with (5), we can obtain the coupling coefficient as:

$$k_m = \left\{ \frac{Z_0}{L_0} \left(\frac{1}{\omega_c} - \frac{\omega_c}{\omega_0^2} \right) \right\}^{1/2}. \quad (9)$$

The equivalent circuit parameters are calculated for various radii of the etched circular pattern and the results are summar-

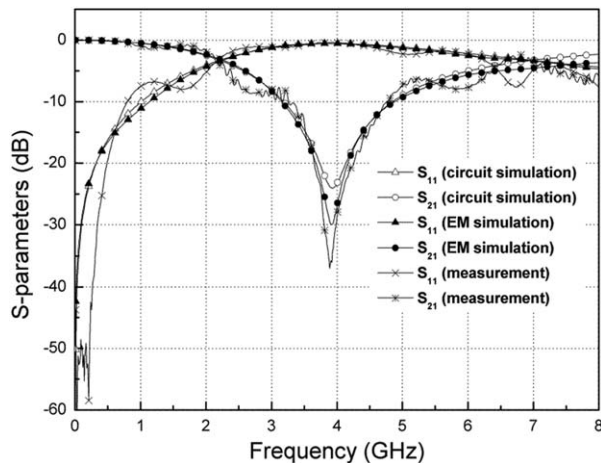


Figure 5 Comparison of S -parameters by circuit simulation (ADS), EM simulation (HFSS), and measurement

ized in Table 1. In the design, a circuit board RO3010 with a dielectric constant of 10.2, copper thickness of 0.016 mm and substrate thickness of 1.27 mm is used. The characteristic impedance of the transmission line was designed to be 50 Ω ($w = 1.2$ mm) and the gap width of DGS was $g = 0.4$ mm. To obtain L_d and C_d , we chose the value of C_r for loaded DGS as 0.1 pF and the simulation is performed using the HFSS.

From the calculated data in Table 1, one can clearly observe that the increase in the radius of the etched circular pattern causes an increase in the coupling coefficient k_m . Also, it can be seen that values of both L_d and C_d , calculated using (4), become larger as the etched circular pattern radius increases. For DGS in the ground plane, the narrow etched gap is not the sole source of the capacitance. Quite obviously, the charges on the ground plane surrounding the circular etched pattern also play a role in providing the surface capacitance. Therefore, C_d is the sum of gap capacitance and surface capacitance. The surface capacitance increases as the dimension of etched circular pattern grows, and the resulting value of C_d increases. Also, from Table 1, it is seen that the value of resistance R_d slowly increases as the radius of the etched circular pattern increases.

Figure 5 illustrates the comparative S -parameters from the simplified equivalent circuit simulation (ADS), the EM simulation (HFSS), and the measurement for a fabricated DGS with $r = 4$ mm. The comparison results show that the proposed circuit model provides a reasonable accuracy.

4. CONCLUSION

This paper has presented a new equivalent circuit model for a dumbbell-shaped DGS and simple DGS structure loaded with capacitance to extract the inductance and the capacitance of the DGS in the ground plane. Also, the main parameters of the proposed equivalent circuit are calculated for various etched circular pattern radii using EM simulation results. The proposed

analysis will provide one approach to understand the electromagnetic behavior of the dumbbell-shaped DGS.

REFERENCES

1. D. Ahn, J.S. Park, C.S. Kim, J.N. Kin, Y. Qian, and T. Itoh, A design of the low-pass filter using the novel microstrip defected ground structure, *IEEE Trans Microwave Theory Tech* 49 (2001), 86–93.
2. I.S. Chang and B.S. Lee, Design of defected ground structures for harmonics control for active microstrip antenna, In: *Proceedings of IEEE Antennas Propagation Society International Symposium*, San Antonio, TX, 2002, pp. 852–855.
3. J.S. Lim, J.S. Park, Y.T. Lee, D. Ahn, and S.W. Nam, Application of defected ground structure in reducing the size of amplifiers, *IEEE Microwave Wireless Compon Lett* 12 (2002), 261–263.
4. D.J. Woo and T.K. Lee, Suppression of harmonics in Wilkinson power divider using dual-band rejection by asymmetric DGS, *IEEE Trans Microwave Theory Tech* 53 (2005), 2139–2144.
5. C. Caloz, H. Okabe, T. Twai, and T. Itoh, A simple and accurate model for microstrip structures with slotted ground plane, *IEEE Microwave Wireless Compon Lett* 14 (2004), 133–135.
6. A. Abdel-Rahman, A. Boutejdar, A.K. Verma, G. Nadim, and A.S. Omar, Improved circuit model for DGS based lowpass filter, In: *Proceedings of IEEE Antennas Propagation Society International Symposium*, Monterey, CA, 2004, pp. 998–1001.
7. N. Karmakar, S. M. Roy, and I. Balbin, Quasi-static modeling of defected ground structure, *IEEE Trans Microwave Theory Tech* 54 (2006), 2160–2168.
8. A.M.E. Safwat, S. Tretyakov, and A.V. Raisanen, Defected ground and patch-loaded planar transmission lines, *IET Microwaves Antennas Propag* 5 (2009), 195–204.
9. C.H. Cheng, C.H. Tasi, and T. L. Wu, A novel time domain method to extract equivalent circuit model of patterned ground structures, *IEEE Microwave Wireless Compon Lett* 20 (2010), 486–488.
10. K.B. Jung, J.K. Lee, Y.C. Chung, and J.H. Choi, Circuit model analysis for traces that cross a DGS, *J Electromagn Eng Sci* 12 (2012), 240–246.
11. D.J. Woo, T.K. Lee, and J.W. Lee, Equivalent circuit model for a simple slot-shaped DGS microstrip line, *IEEE Microwave Wireless Compon Lett* 23 (2013), 447–449.
12. E.O. Hammerstad, Equations for microstrip circuit design, In: *5th European Microwave Conference*, Hamburg, Germany, 1975, pp. 268–272.

© 2014 Wiley Periodicals, Inc.

INTENSITY MODULATION USING CHIRPED FIBER BRAGG GRATING AS AN EDGE FILTER FOR TEMPERATURE SENSING

Deepa Srivastava, Randhir Bhatnagar, Asha Kumar, and Vinod Parmar

Advanced materials and Sensors, Central Scientific Instruments Organisation (Council of Scientific and Industrial Research, New Delhi), Chandigarh, 160030, India; Corresponding author: deepa@csio.res.in

Received 21 April 2014

ABSTRACT: We demonstrate a prominent technique using intensity variation owing to a change in temperature of fiber Bragg grating (FBG) instead of just a shift of Bragg wavelength due to ambient temperature variation. The rising and falling region of chirped fiber Bragg grating (CFBG) spectrum can be used as edge filter, where intensity variation can be observed with the shift in wavelength due to change in temperature. The proposed hypothesis of intensity variation with a shift in wavelength at rising edge of CFBG has been investigated theoreti-

cally and later on these results are verified experimentally. The rising and falling edge of CFBG are analyzed and then FBG was written on 1542.4 nm. The rising edge of CFBG have linear region in the range of 1542.3–1542.7 nm wavelength. Thus intensity will be modulated linearly with a shift of Bragg wavelength in this region. In-house fabricated FBG has been used and CFBG as an edge filter was implemented in our experiment to verify the proposed concept of intensity modulation. © 2014 Wiley Periodicals, Inc. *Microwave Opt Technol Lett* 56:2913–2915, 2014; View this article online at wileyonlinelibrary.com. DOI 10.1002/mop.28737

Key words: fiber Bragg grating; chirped fiber Bragg grating; interrogation techniques; amplified spontaneous emission

1. INTRODUCTION

Fiber Bragg grating (FBG) based sensors have many advantages in contrast to conventional electrical and alternative fiber optic sensors in terms of economical production cost, immune to electromagnetic interference, light weight, and minuscule in size for compact packaging. FBGs are used as sensing elements for the measurement of physical parameters, such as strain, temperature, and pressure [1,2]. Transition in these physical parameters leads to a shift in Bragg wavelength of FBG which is measured using various wavelength interrogation techniques. Many interrogation techniques based on Fabry–Perot filter, acousto-optic tunable filter, matched FBG pair, edge filter based, Mach–Zehnder interferometer, CCD spectrometer, and fiber Fourier transform spectrometer are already reported [2]. The edge filter based interrogation technique is used in our study for wavelength-to-intensity linear conversion for sensing. This technique is better as compared to other techniques in terms of quick sensing, sensing temperature range, and development cost. Various edge filter have been used in interrogation system such as biconical fiber filters [3], thin film filter [4], single-multimode-single through multimode interference [5], Macrobending fiber based filter [6], LPG [7] amplified spontaneous emission (ASE) profile as an edge filter [8], WDM Couplers [9], and chirped fiber Bragg grating (CFBG) [10,11].

In this article, we report theoretical results of intensity variation with respect to Bragg wavelength shift using CFBG as an edge filter. Furthermore, these results are experimentally verified to propose CFBG as an edge filter.

2. THEORY

The FBG is fabricated in the core of a germanium doped single-mode optical fiber using spatially-varying pattern of intense UV laser light. The UV light has sufficient energy to break the highly stable silicon-oxygen bonds in the optical fiber and thereby increasing its refractive index slightly more than the nongrating areas. A periodic spatial variation in intensity of UV light caused by the interference of two coherent beams or a mask placed over the fiber, gives rise to a corresponding periodic variation in the refractive index of the fiber. The grating formed at this modified region of fiber becomes a wavelength selective filter. Light propagating in this portion of fiber is partially reflected by each of the tiny index variations, but these reflections interfere destructively at most of the wavelengths. However, depending on the pitch of grating and effective refractive index of fiber, at one particular narrow range of wavelengths constructive interference occurs and light is reflected back in the fiber. Bragg wavelength (λ_B) is defined by given equation